Nano Express

In-situ observation of nucleation and property evolution in films grown with an atmospheric pressure spatial atomic layer deposition system

IOP Publishing Nano Express 1 (2020) 010045 https://doi.org/10.1088/2632-959X/ab976c

NANO EXPRESS

PAPER

In-situ observation of nucleation and property evolution in films grown with an atmospheric pressure spatial atomic layer deposition system

Kissan Mistry[1,2], **Alexander Jones**[1,2], **Manfred Kao**[1,2], **Travis Wen-Kai Yeow**[1,2], **Mustafa Yavuz**[1,2] and **Kevin P Musselman**[1,2]

[1] Waterloo Institute for Nanotechnology, University of Waterloo, Waterloo, N2L 3G1, Canada
[2] Department of Mechanical and Mechatronics Engineering, University of Waterloo, Waterloo, N2L 3G1, Canada

E-mail: kevin.musselman@uwaterloo.ca

OPEN ACCESS

RECEIVED
6 April 2020

REVISED
20 May 2020

ACCEPTED FOR PUBLICATION
28 May 2020

PUBLISHED
9 June 2020

Keywords: *in-situ* characterization, reflectometry, open-air, chemical vapor deposition, spatial atomic layer deposition, aluminum oxide, zinc oxide

Supplementary material for this article is available online

Abstract

Atmospheric pressure—spatial atomic layer deposition (AP-SALD) is a promising open-air deposition technique for high-throughput manufacturing of nanoscale films, yet the nucleation and property evolution in these films has not been studied in detail. In this work, *in situ* reflectance spectroscopy was implemented in an AP-SALD system to measure the properties of Zinc oxide (ZnO) and Aluminum oxide (Al_2O_3) films during their deposition. For the first time, this revealed a substrate nucleation period for this technique, where the length of the nucleation time was sensitive to the deposition parameters. The *in situ* characterization of thickness showed that varying the deposition parameters can achieve a wide range of growth rates (0.1–3 nm/cycle), and the evolution of optical properties throughout film growth was observed. For ZnO, the initial bandgap increased when deposited at lower temperatures and subsequently decreased as the film thickness increased. Similarly, for Al_2O_3 the refractive index was lower for films deposited at a lower temperature and subsequently increased as the film thickness increased. Notably, where other implementations of reflectance spectroscopy require previous knowledge of the film's optical properties to fit the spectra to optical dispersion models, the approach developed here utilizes a large range of initial guesses that are inputted into a Levenberg-Marquardt fitting algorithm in parallel to accurately determine both the film thickness and complex refractive index.

1. Introduction

Atmospheric pressure—spatial atomic layer deposition (AP-SALD) is an emerging technique that is capable of producing conformal, pinhole-free films in open-air. Whereas conventional atomic layer deposition (ALD) operates by sequentially inserting two chemical precursor gases into a vacuum chamber, with evacuation and purge steps in between (precursors are separated in time), AP-SALD separates the precursors in space. Figure 1 illustrates the close-proximity AP-SALD approach, where a substrate is placed very close (~100 micrometers) to a reactor head that contains parallel slits with flows of two precursor gases. The substrate can be oscillated back and forth underneath the reactor to replicate the sequential gas exposure steps and deposit a film one atomic layer at a time. The AP-SALD approach eliminates the evacuation and purge steps that make conventional ALD slow, and it does not require a vacuum chamber, which makes it scalable and potentially less costly. Furthermore, by adjusting the reactor-substrate spacing and/or flow rates, the system can deposit by chemical vapor deposition('CVD mode') [1], where some mixing of the precursors occurs in the gas phase. This atmospheric pressure chemical vapor deposition (AP-CVD) generally results in accelerated film deposition rates, while still producing conformal, pinhole-free films [2]. Growing interest in spatial ALD has led to several review papers in recent years [3–6], and companies such as Levitech, Beneq, and SoLayTec have commercialized

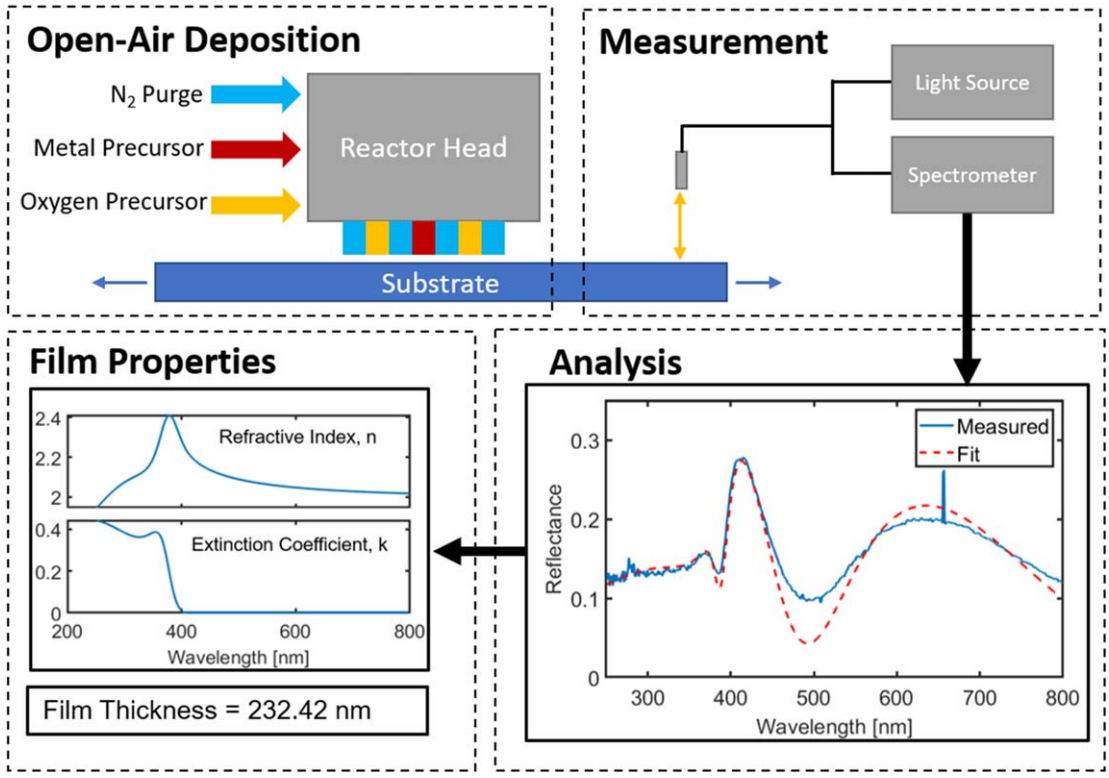

Figure 1. Schematic overview (not to scale) of the implemented method consisting of thin film deposition, measurement, analysis, and determination of film properties. Deposition in open-air was performed by AP-SALD utilizing a 'close-proximity' reactor head. The film is grown on the substrate that oscillates underneath the reactor head. Concurrently, reflectance spectra of the growing film are captured by the mounted reflectance probe and spectrometer. Each spectrum is fitted to optical models to obtain the film thickness and the refractive index (***n***) and extinction coefficient (imaginary part of refractive index, ***k***).

spatial ALD systems. Both metal oxides and metals have been deposited [4, 5, 7], and AP-SALD and AP-CVD films have been utilized in thin film transistors [8, 9], metal-insulator-metal diodes [10], photovoltaic devices [2, 11–17], and LEDs [18–20]. Yet despite the promise of these techniques, little has been done to characterize the nucleation and property evolution of these nanoscale films. This may follow, in part, from the expectation that the chemistry and film formation is identical to conventional ALD, which neglects the influence of atmospheric conditions (i.e. open-air). It was recently shown, for example, that the periodic exposure of Al:ZnO films to oxygen during deposition in an AP-SALD system results in a higher trap density at grain boundaries, which limits the electron mobility [21]. As for other nanoscale film deposition methods, an understanding of film nucleation and property evolution is necessary to permit the fabrication of AP-SALD and AP-CVD films with specific properties and desired thickness and morphology.

In-situ characterization techniques are typically used to study film nucleation and evolution. Quartz crystal microbalances which are commonly used to measure film deposition rates, are unsuitable for the AP-SALD arrangement shown in figure 1, as are reflection high energy electron diffraction (RHEED) methods employed in ultra-high vacuum environments [22–25]. Conventional ALD systems typically employ spectroscopic ellipsometry for the determination of film thickness and optical properties [26]. However, the arrangement of the optics involved tend to be 'bulky' and is not ideal to make multiple real time measurements across the substrate area. Other optical spectroscopy techniques can be more easily integrated into AP-SALD systems. Mione *et al* [27] recently used infrared and optical emission spectroscopy to study the gas-phase chemistry of aluminum oxide (Al_2O_3) deposition in an atmospheric-pressure plasma-enhanced SALD system. Yersak *et al* [28] used *in situ* reflectance spectroscopy to monitor the growth of insulating Al_2O_3 films deposited by a continuous web AP-SALD system. A reflectance probe was mounted above the polymer web substrate and continuously captured reflectance spectra throughout the growth. Known Al_2O_3 refractive index values were inputted into commercial software which used the Cauchy dispersion model to determine the thickness of the deposited film, although accurate thicknesses below 20 nm could not be measured and hence this technique could not be used to study the nucleation behavior of films.

In this work, an advanced reflectance spectroscopy characterization tool is developed and implemented into an AP-SALD system. Using this characterization tool, the nucleation and property evolution of insulating (Aluminum Oxide, Al_2O_3) and semiconducting (Zinc Oxide, ZnO) thin films deposited with an AP-SALD

system (operated in AP-CVD conditions) are observed for the first time. Superior measurements at low thicknesses enable the direct observation of a substrate nucleation phase prior to film deposition, as well as the effect of different deposition parameters on this nucleation phase. The evolution of the complex refractive index can be observed throughout film deposition, and it is found that by changing the deposition parameters, the film nucleation can be controlled to produce ZnO films with different bandgaps and Al_2O_3 films with different refractive indices.

2. Experimental

Film deposition was performed using a custom-built AP-SALD system, which employs a close-proximity reactor head configuration as described elsewhere [4, 6, 29]. Briefly, liquid precursors are bubbled with an inert gas (Nitrogen, N_2) that carries the precursor vapors to the reactor head. Before they arrive at the reactor head, they combine with additional streams of inert gas at higher flow rates that serve to push the precursors to the reactor (carrier lines). The ratio between the flow rate of the bubbler and the flow rate of the carrier line is used to represent the concentration of the precursor in the line, however, the actual concentration would be lower. As illustrated by the 'Open-Air Deposition' section of figure 1, flows of metallic and oxygen precursors are fed into the reactor head which subsequently distributes the flows into an alternating sequence of spatially separated parallel channels. In between the precursor channels exists N_2 purging and exhaust (not shown) channels. A vacuum pump was connected to the exhaust channels to actively exhaust any unreacted precursor. The reactor head is held a set distance above the heated substrate stage. Larger reactor-substrate separation heights reduce the effectiveness of the purging and exhaust channels and therefore allow intermixing of the precursors before deposition onto the substrate, analogous to chemical vapor deposition (AP-CVD mode). A single deposition cycle by AP-SALD consists of one complete oscillation (back and forth movement) of the substrate stage. This represents 2 conventional ALD cycles.

Insulating Al_2O_3 films were deposited on silicon wafers, using trimethylaluminum (TMA) as the metallic precursor and water as the oxygen precursor. The outlet channel flow rate was set to 125 SCCM with a metal precursor concentration of 30% and an oxygen precursor concentration of 60%. The substrate temperature was varied from 100 °C–250 °C in increments of 50 °C and the oscillation speed was varied from 15–50 mm s^{-1}. Semiconducting ZnO films were deposited on borosilicate glass, using diethylzinc (DEZ) as the metallic precursor and water as the oxygen precursor. The outlet channel flow rate was set to 150 SCCM with both the metallic and oxygen precursor concentrations set to 15% unless otherwise specified. These deposition conditions are similar to those previously reported to result in AP-CVD film growth [2]. The substrate temperature was varied from 50 °C–200 °C in increments of 50 °C and the substrate oscillation speed was varied from 5–50 mm s^{-1}. The substrates were rinsed with isopropyl alcohol and dried with compressed air before placing on the heated substrate stage for 2min to arrive at the correct deposition temperature. In both cases, the reactor-substrate separation was set to 100 μm.

As shown in the 'Measurement' section of figure 1, a bifurcated reflectance probe is mounted above the substrate stage at normal incidence (Ocean Optics QR600). A UV-Visible light source (Ocean Optics DH-2000) coupled to the reflectance probe was used to illuminate the surface of substrate. Reflected light is directed back to the reflectance probe and captured by the UV-Visible spectrometer (Ocean Optics HDX-UV–vis) with a range of 250–800nm. Calibration of the reflectance measurement requires the measurement of the background (bare substrate), the noise in the system (dark measurement) and the measurement of a known standard (silicon). For measurements of films grown on borosilicate glass, a matte black tape was used to cover the metallic stage to remove unwanted backside reflections. The spectrometer acquisition time was set using a modified exponential search algorithm to optimize the light intensity range for the spectrometer's detector [30], resulting in acquisition times that were typically less than 6 milliseconds. Reflectance spectra were captured every two deposition cycles in the same spot.

The determination of film properties is done by fitting the measured reflectance spectrum to an optical reflectance model. This model (figure S1 in the supplementary material is available online at stacks.iop.org/NANOX/1/010045/mmedia) consists of a three-layer stack (air-film-substrate) whose total reflectance is governed by the Fresnel reflectance equations (equations (1)–(8) in the supplementary material). Parameters of importance are the complex refractive indices of each layer and thickness of the growing film [31]. The complex refractive index is comprised of the real component n and the imaginary component k, also referred to as the extinction coefficient. The refractive indices of air and the substrate are known parameters, while the wavelength (λ)-dependent complex refractive index and the thickness of the film are unknowns. For Al_2O_3 and other non absorbing films, the refractive index can be described by the Cauchy dispersion model [31] where $n(\lambda)$ is a function of 3 fitting parameters and $k(\lambda) = 0$ (equations (9)–(10) in the supplementary material). Including thickness, there are a total of 4 fitting parameters used to fit the measured spectrum to the reflectance model. The

Tauc-Lorentz dispersion model is used for polycrystalline semiconductors such as ZnO [32, 33]. Here, 9 fitting parameters are used to determine the film's complex dielectric function from which $n(\lambda)$ and $k(\lambda)$ can be obtained and results in a total of 10 fitting parameters to fit the measured reflectance spectrum (equations (11)–(12) in the supplementary material).

A Levenberg-Marquardt (LM) fitting algorithm is used to fit the previously unknown parameters in the reflectance models to the measured reflectance spectra to simultaneously determine both the film's complex refractive index and thickness. The built-in function *lsqcurvefit* in MATLAB was used to perform the Levenberg-Marquardt (LM) fitting [34]. The function returns a goodness of fit (GOF) which is simply the R-square value. Where other implementations of reflectance fitting require previous knowledge of the film's optical properties to be used as initial guesses, the implementation discussed here makes use of several guesses in a range inputted in parallel into the LM algorithm, such that previous knowledge of the film's optical properties is not used. For both the Cauchy and Tauc-Lorentz fit parameters an initial guess value of 1 was used. For the thickness parameter, several guesses in a range centred around the deposition cycle number were inputted in parallel to the *lsqcurvefit* function, from which the fit with the highest GOF was selected. This was done to account for the tendency of LM fitting programs to minimize to the local minima instead of the global minima resulting in erroneous values. This method is found to be quite successful in measuring the overall growth behavior of a deposited film. However, inaccurate fitting results occasionally occur and are represented by large spikes in the thickness values that deviate from the overall growth rate. For these cases, the incorrect thickness is corrected by refitting the spectrum using the fit parameters of the deposition cycles before and after the incorrect point. Furthermore, to improve accuracy of low thickness fits, a smaller range of parallel guesses was used ($\pm$5 nm) until the film thickness reached 30nm after which the range was extended ($\pm$ 50 nm). The thickness of films, as determined by reflectance spectroscopy, matched closely with the thickness measured by spectroscopic ellipsometry (J.A. Woollam M-2000DI). This validated the method described herein for the *in situ* thickness measurement of films deposited by AP-SALD. As shown in the 'Film Properties' section of figure 1, the LM fitting algorithm returns the film's thickness, and refractive index, as well as the extinction coefficient for semiconductors. Consequentially, the absorption coefficient (α) can be determined and the optical bandgap identified using the well known Tauc equation [35, 36] (equations (16)–(17) in the supplementary material). A direct bandgap ($r = 1/2$) was assumed for ZnO films [37–39].

The effect of film roughness can be accounted for by introducing an additional layer in between the air and film layers of the optical model. The thickness of this layer is equated to the RMS roughness of the film, while the optical properties of the layer are described by the Bruggeman effective medium approximation [40, 41]. Due to the increased complexity of the four-layer model and its longer computation fitting time, the effect of roughness was omitted in this work. This was justified by comparing the fitting results between the four- and three-layer models (shown in figure S2 of the supplementary material), which showed negligible differences. Furthermore, it was previously shown that the optically determined roughness of the film often does not reflect the true roughness of the film as determined by atomic force microscopy [41, 42].

3. Results and discussion

Video S1 and S2 (available online at stacks.iop.org/NANOX/1/010045/mmedia) included in the supplementary material show the measured and fitted reflectance spectra for ZnO and Al_2O_3 films during their deposition, and the evolution of the film thickness and optical properties. A summary of these videos is illustrated in figure 2 Measured reflectance spectra are shown in figures 2(a) and (d) for ZnO and Al_2O_3, respectively. The thickness of the film at each measured cycle is plotted (figures 2(b) and (e)) and can be used to determine the growth rate per cycle (GPC). The goodness of fit is also shown. The real part of the refractive index at a wavelength of 600nm is shown as a function of deposition cycles and is relatively consistent throughout the deposition (figures 2(c) and (f)). For ZnO, the bandgap of the growing film is also shown (figure 2(c)).

3.1. Film Nucleation and Growth

Figure 3(a) shows the obtained thickness of ZnO films deposited at three different substrate oscillation speeds (15, 30 and 50 mm s^{-1}). Here, substrate oscillation speed is inversely related to the precursor dose or exposure time that is typically referenced in conventional ALD literature. The substrate stage moving at a lower speed gives the precursors more time to adsorb and react on the surface of the substrate. As depicted in figure 3(a), film growth is found to occur in two stages: a nonlinear surface nucleation/incubation stage and a linear growth stage. This growth behavior is consistent with that of conventional vacuum based ALD, which has been verified by *in situ* crystal microgravimetry(QCM) [22], scanning electron microscopy(SEM) [43], atomic force microscopy(AFM) [44], and surface profilometry [45]. The lack of growth during the initial deposition cycles is attributed to the nucleation time to form ZnO nuclei on the bare substrate [22]. The density of ZnO nuclei

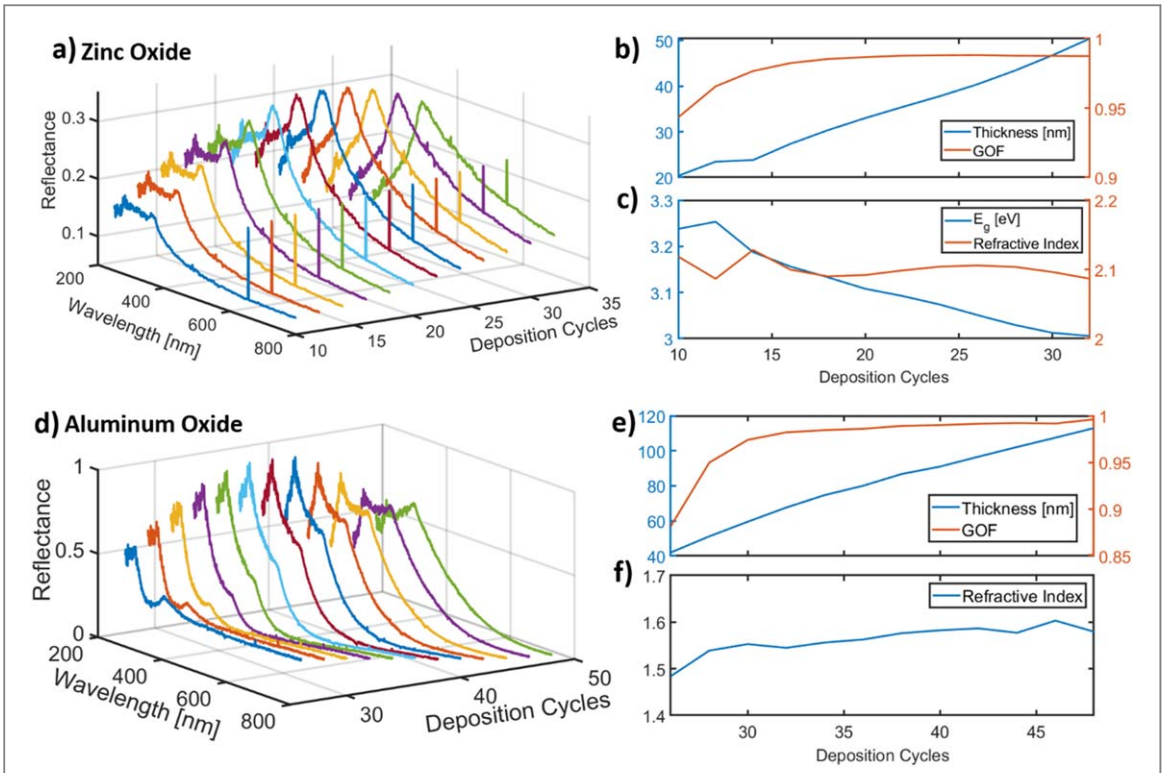

Figure 2. Reflectance spectra measured every 2 deposition cycles and the respective determined thickness and optical properties. (a) ZnO reflectance spectra from 10–30 cycles. (b) ZnO film thickness (left) and goodness of fit (right). (c) ZnO optical bandgap, E_g $[eV]$ (left), and refractive index at 600nm (right). (d) Al_2O_3 reflectance spectra from 20–50 cycles. (e) Al_2O_3 film thickness (left) and goodness of fit (right). (f) Al_2O_3 refractive index at 600nm.

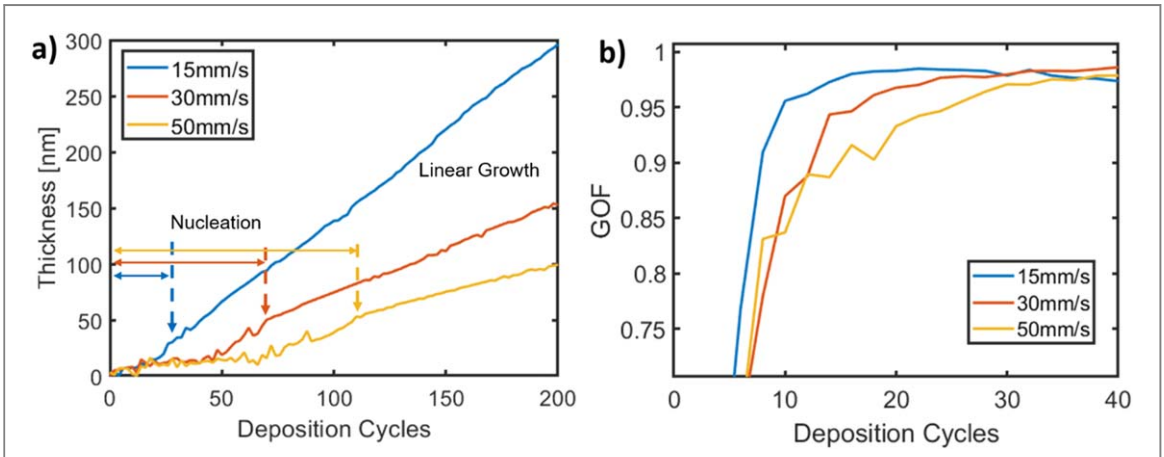

Figure 3. Growth of ZnO thin films at T = 150 °C at three different stage oscillation speeds. (a) Thickness of ZnO as a function of deposition cycles. Arrows indicate the length of the 'surface nucleation' window for each oscillation speed. (b) Goodness of fit for ZnO reflectance spectra measured for the first 40 deposition cycles.

created is related to the amount of adsorbed hydroxyl groups on the surface. The precursors will readily adsorb and react with the ZnO nuclei (active sites) resulting in an island-like growth. This continues until the islands eventually coalesce forming a complete layer, after which layer by layer growth behavior occurs in a linear fashion. This two-stage growth mechanism has been extensively reviewed by R.L. Puurunen who states that many ALD growth studies inaccurately claim a full monolayer per cycle growth from the start but that this has never been experimentally verified [46]. Methods to decrease nucleation time have included substrate pre-treatment with oxygen plasma [43] or acid cleaning [45] to increase the hydroxyl density on the surface. More commonly, increasing the length of the precursor dose time results in an increase in ZnO nuclei formation consequently decreasing the nucleation time [44]. This effect has been reproduced by AP-SALD here, where it is seen in figure 3(a) that depositions done with quicker oscillation speeds and hence lower precursor dose times,

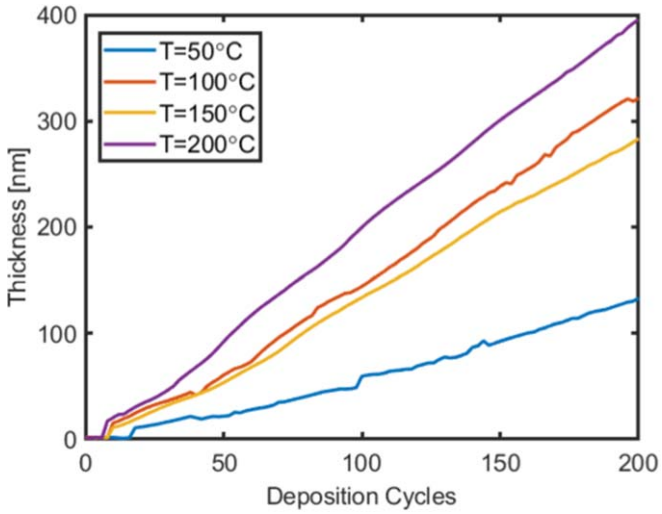

Figure 4. ZnO film thickness at varying deposition temperatures with a substrate oscillation speed of 5 mm s^{-1}. Similar plots for other substrate oscillation speeds are presented in figure S4 in the supplementary material. The results are summarized in tables 1 and 2.

Table 1. Nucleation period (number of cycles) for ZnO thin films deposited with varying temperatures and substrate oscillation speeds.

	50 °C	100 °C	150 °C	200 °C
5 [mm s^{-1}]	34	14	10	8
15 [mm s^{-1}]	70	32	24	18
30 [mm s^{-1}]	98	46	40	34
50 [mm s^{-1}]	120	64	58	44

require more deposition cycles to populate the surface with ZnO nuclei that subsequently grow into a continuous film and enter the linear growth regime.

The goodness of fit of the obtained reflectance spectra is shown in figure 3(b) where a similar trend is observed in that quicker oscillation speeds require more deposition cycles to obtain a high GOF (>0.9) corresponding to the formation of a complete film layer on the substrate. These results show that linear growth rates cannot be assumed from the first deposition cycle, which becomes particularly releveant in thin film applications such as passivation layers and transparent coatings. The *in situ* reflectance spectroscopy technique introduced in this work enables the deposition of nanoscale films with accurate thickness.

Control of the ZnO film nucleation and growth rates was further explored by introducing the deposition temperature as an additional parameter. ZnO films were deposited on borosilicate glass at temperatures of 50, 100, 150 and 200 °C, with substrate oscillation speeds of 5,15, 30 and 50 mm s^{-1} for a total of 16 ZnO samples in the study. Each film was deposited for 200 cycles, with *in situ* reflectance measurements taken every 2 cycles. To obtain the same dataset by an *ex situ* measurement technique would require the deposition of 1600 individual ZnO samples. Figure 4 compares the measured thicknesses of ZnO films deposited at different temperatures for an oscillation speed of 5 mm s^{-1}. Similar thickness plots for other oscillation speeds are presented in figure S4 in the supplementary material. The growth behavior results of the total study are summarized in table 1 (nucleation period) and table 2 (linear growth rates).

Table 1 shows that an increase in deposition temperature results in a decrease in the number of cycles to saturate the surface of the substrate. This is in contrast to the nucleation behavior of ZnO in conventional chamber-based ALD, where higher temperatures result in desorption of the precursors from the substrate and therefore require longer nucleation times [46]. The deviation from this behavior is attributable to the high-pressure open-air environment of AP-SALD which has an abundance of oxygen and hydroxyls, as well as the use of parameters that are expected to result in chemical vapor deposition. In agreement with the results obtained here, AP-CVD of ZnO films by Biswas *et al* showed that substrate coverage can be significantly improved by increasing growth temperatures [47]. This is because the elevated temperatures accelerate precursor gas phase reaction in air, rather than adsorption on the substrate, resulting in shorter nucleation times and quicker growth rates [48].

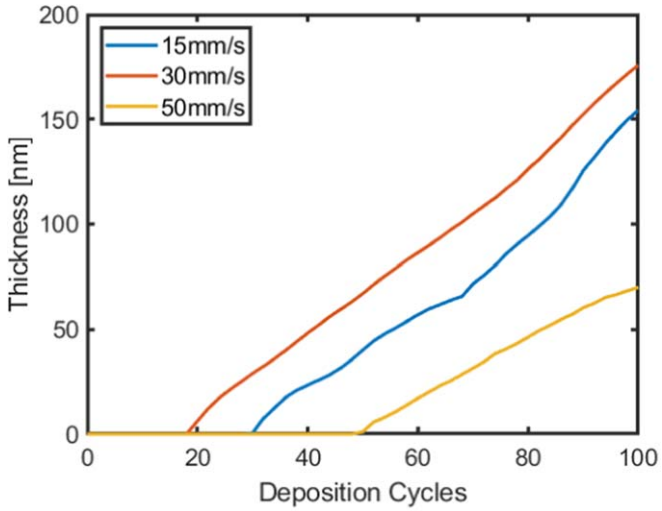

Figure 5. Thickness of deposited Al_2O_3 film at varying substrate oscillation speeds with a deposition temperature of 200 °C. Thickness plots of Al_2O_3 films deposited at other temperatures are presented in the supplementary material. The results are summarized in tables 3 and 4.

Table 2. Linear growth rates per cycle (nm/cycle) for ZnO thin films deposited with varying temperatures and substrate oscillation speeds. One AP-SALD cycle corresponds to 2 conventional ALD cycles.

	50 °C	100 °C	150 °C	200 °C
5 [mm s^{-1}]	0.62	1.68	1.48	2.03
15 [mm s^{-1}]	0.27	0.51	0.62	1.47
30 [mm s^{-1}]	0.18	0.30	0.35	0.32
50 [mm s^{-1}]	0.10	0.18	0.35	0.29

The data presented in table 2 demonstrate that a wide range of growth rates of 0.1–2 nm/cycle (corresponding to 0.05–1 nm per conventional ALD cycle) are achievable. An increase in deposition temperature generally results in an increase in growth rate per cycle. This is in agreement with the shorter nucleation times observed at higher temperature. The growth rate is seen to decrease as the substrate oscillation speed increases (dose time decreases). Despite operating with parameters that are expected to result in AP-CVD, the growth rates at oscillation speeds of 30 and 50 mm s^{-1} are comparable to ZnO growth rates achieved by conventional ALD of 0.1–0.3 nm per ALD cycle [4, 49–51]. Decreasing the oscillation speed to 15 or 5 mm s^{-1} resulted in an increase in growth rates up to 2 nm/cycle (1 nm per ALD cycle), consistent with AP-CVD, where the slower oscillation speed allows for a longer AP-CVD reaction [48]. There are a few minor deviations from the noted trends in table 2: GPC at 100 °C versus 150 °C for an oscillation speed of 5mm s^{-1}, and, 150 °C versus 200 °C for oscillation speeds of 30 mm s^{-1} and 50mm s^{-1}. Since many of these depositions occurred one after another, one possible explanation to the higher growth rate at a lower temperature can be due to an accumulation of precursor in the line. Additionally, the spacing between the stainless-steel reactor head and the substrate was manually set to 100μm at the start of the study. It is possible that at the lower temperature the substrate thermally expanded less and therefore resulted in a spacing that was larger than 100μm and promoted more precursor mixing resulting in the higher growth rate. Another possible explanation lies in classical ALD theory, where higher deposition temperatures outside of the 'ALD window' result in desorption of the precursor from the substrate [52–55]. This phenomena may be more relevant to higher growth rates at 150 °C than 200 °C for both 30 and 50 mm s^{-1} oscillation speeds, whereas the anomaly observed at 100 °C versus 150 °C is most likely due to the previous two explanations.

A similar study to examine the influence of deposition parameters was done for Al_2O_3 films. Al_2O_3 films were deposited at temperatures of 100, 150, 200 and 250 °C with oscillation speeds of 15, 30 and 50 mm s^{-1} on silicon substrates (12 samples in total, 100 cycles each). Figure 5 compares the measured thickness of films deposited at 200 °C for different oscillation speeds. Similar thickness plots for other deposition temperatures are presented in figure S4 in the supplementary material. The growth behavior results of the total study are summarized in table 3 (nucleation period) and table 4 (linear growth rate). While the growth behavior for ZnO

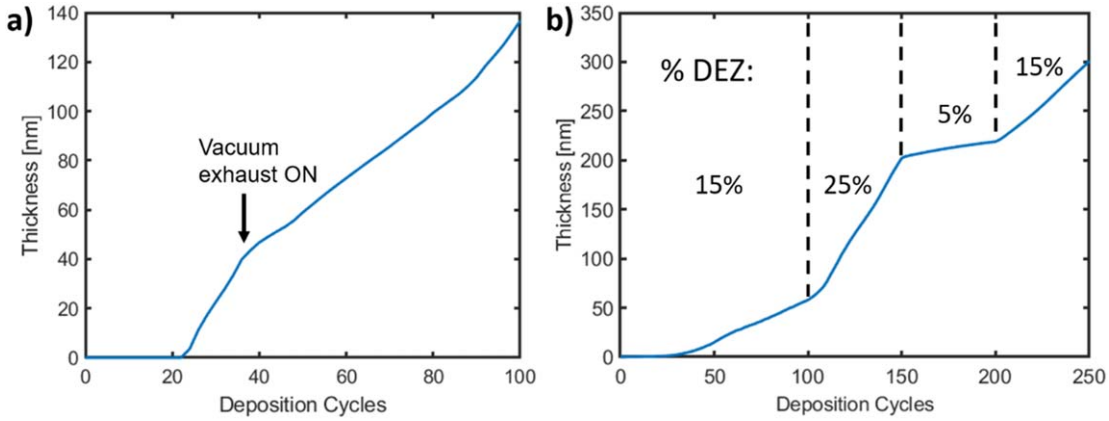

Figure 6. Real time monitoring of deposition errors and rate. (a) Thickness of a deposited Al_2O_3 film (T = 150 °C), the vacuum pump for the exhaust channels was not turned on for the first 36 deposition cycles. (b) Different deposition rates for a ZnO film (T = 200 °C), the DEZ flow rates were varied.

Table 3. Nucleation period (number of cycles) for Al_2O_3 thin films deposited with varying temperatures and substrate oscillation speeds.

	100 °C	150 °C	200 °C	250 °C
15 [mm s^{-1}]	18	24	30	16
30 [mm s^{-1}]	10	52	18	24
50 [mm s^{-1}]	74	22	50	18

Table 4. Linear growth rates per cycle (nm/cycle) for Al_2O_3 thin films deposited with varying temperatures and substrate oscillation speeds. One AP-SALD cycle corresponds to 2 conventional ALD cycles.

	100 °C	150 °C	200 °C	250 °C
15 [mm s^{-1}]	1.68	1.47	2.28	2.92
30 [mm s^{-1}]	1.13	1.21	2.11	1.57
50 [mm s^{-1}]	1.09	0.83	1.44	0.78

closely followed the expected trends, this is not the case for Al_2O_3. For example, as shown in figure 5, the nucleation period is larger for an oscillation speed of 15mm s^{-1} compared to 30 mm s^{-1}, where the opposite would be expected. There are no clear trends in the nucleation period, as presented in table 3. Additionally, the rates presented in table 4 do not exhibit clear trends in growth behavior. As reported previously, the atmospheric ('open-air') deposition of Al_2O_3 using the highly pyrophoric precursor TMA, can be challenging to reproduce [56]. The ambient oxygen and water in the air (humid conditions) can act as an additional oxygen source that can increase growth rates [57]. Human error in adjusting the reactor head spacing can lead to an overmixing of the precursors (AP-CVD) and deposition with high rates [5]. Jur and Parsons concluded that the high pressures of atmospheric deposition will typically increase Al_2O_3 growth rates by ~25%–30% [58]. More importantly, Mousa *et al* noted that at high atmospheric pressures the growth of Al_2O_3 with TMA is largely independent of temperature [59]. It is therefore difficult to observe the influence of temperature and oscillation speed on the Al_2O_3 growth. However, it strongly supports the need for an *in situ* thickness characterization tool for Al_2O_3 grown in atmospheric conditions using this technique.

Added benefits of monitoring the film thickness *in situ* include the ability to monitor for deposition errors and to control the deposition rate. Figure 6(a) depicts an example of error monitoring during the deposition of an Al_2O_3 thin film. The linear growth regime starts after 20 deposition cycles and after 36 cycles the vacuum pump for the exhaust channels was turned on which immediately reduced the growth rate. In this case, the lack of vacuum exhaust during the initial growth period resulted in a higher amount of precursor mixing and consequentially a higher growth rate. Figure 6(b) illustrates the ability to control the deposition rate of a ZnO thin film by varying the precursor (DEZ) flow rate. The initial 100 deposition cycles were done at a concentration

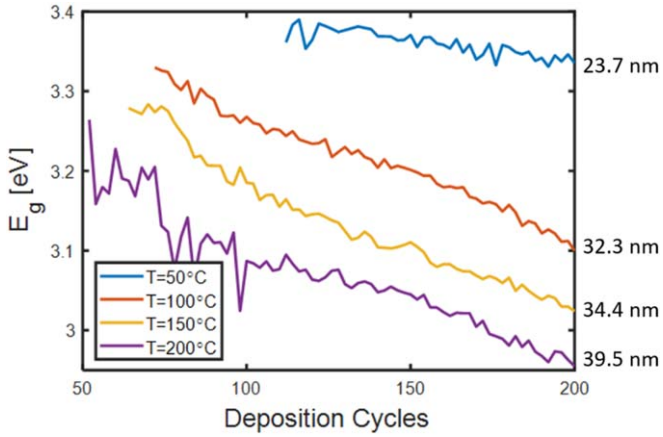

Figure 7. The optical bandgap E_g [eV] of ZnO films obtained from *in situ* reflectance spectroscopy measurements. The influence of deposition temperature on the bandgap is examined throughout the course of film deposition at an oscillation speed of 50 mm s^{-1}. Values are taken after completion of the nucleation period and when high GOF was achieved. Final film thicknesses are listed on the right.

of 15% to first saturate the surface and subsequentially enter the linear growth regime. After 100 cycles the concentration was increased to 25% resulting in a stark increase in the growth rate per cycle. After another 50 cycles the concentration was decreased to 5% resulting in a decrease in growth rate which was followed by an increase in growth rate once the concentration was set back to 15%. The large variation in growth rate is consistent with AP-CVD type growth as discussed earlier.

3.2. Evolution of optical properties

As previously described, the bandgap (E_g) of semiconducting films can be obtained from *in situ* reflectance spectroscopy and thus can be monitored over the deposition period. Figure 7 shows the bandgap evolution of growing ZnO films deposited at different temperatures. The E_g data was taken after the completion of the nucleation period and when high GOF was achieved. As observed in the figure, the obtained bandgaps range from 3.39–2.95 eV, where films deposited at a lower temperature have a higher initial bandgap. This is consistent with previous reports, where three reasons are presented. The first attributes the bandgap temperature dependence to the thermal expansion of the ZnO lattice and its direct effect on the relative position of the valence and conduction band [60]. The second is the temperature dependence of the electron-phonon interactions and their affect on the band energies [61]. Lastly, it is known that the higher deposition temperatures result in an increased crystallinity for ZnO films grown by this method, and the decrease in bandgap has been attributed to the improved crystallinity [62]. The bandgap then decreases from the initial value as the film grows which is attributed to the size of the grains as well as the porosity in the nanocrystalline film. The early stages of film growth will consist of smaller crystallite sizes corresponding to higher film porosity. As the film grows the crystallite sizes become larger, the film becomes more compact and the overall film porosity decreases. Like quantum dots, the optical bandgap of a nanocrystalline ZnO film will decrease as the grain size increases [39, 63]. Similarly, the bandgap is expected to decrease as the porosity of the film decreases as well [64, 65]. The general trend of decreasing bandgap as deposition temperature increases has been shown for ZnO films grown by conventional ALD methods [66, 67]. However, values as low as 2.9 eV (deposited at 200 °C) have not, to our knowledge, been reported for ZnO grown by ALD. As described by the Varshini equation [68], the bandgap of semiconductors tends to decrease as a function of the measurement temperature. The sample grown at 200 °C was re-measured at room temperature and had a bandgap of 3.07eV which is still low when compared to that of ALD grown ZnO. This may be attributed to the deposition done in atmospheric conditions, as AP-CVD grown ZnO has reported bandgaps as low as 2.8eV [69].

The refractive index of a thin film can give an indication of film quality and density. Figure 8 shows the refractive index (at 600 nm) of Al_2O_3 films deposited at different temperatures. Values obtained before the completion of the nucleation period were ignored. The initial formation of the films is observed as the refractive index starts at zero or near zero values and increases to a value of 1.4–1.5, which is the expected refractive index range for Al_2O_3 grown by conventional ALD [70, 71]. It is clear that the refractive index of the film grown at 100 °C is lower compared to the films grown at higher temperatures. This is attributed to the decreased density and increased impurity levels of Al_2O_3 grown at lower temperatures [71–73]. It is expected that higher temperatures would promote a higher degree of crystallinity and higher density resulting in an increase in refractive index approaching a value of 1.76, that of sapphire (α-Al_2O_3).

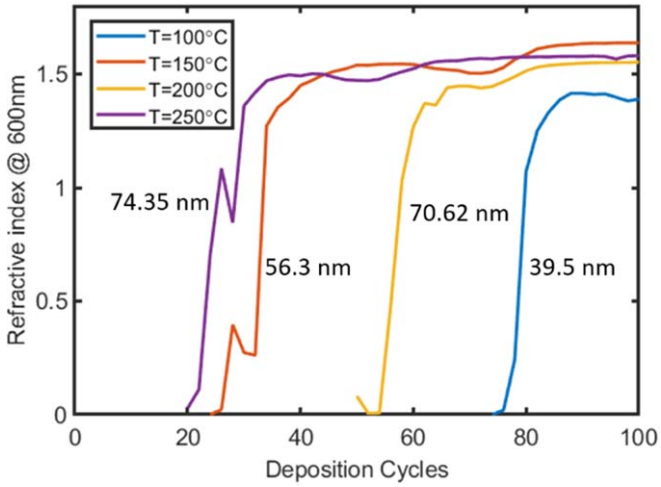

Figure 8. Comparison of refractive index of Al_2O_3 films at different deposition temperatures, as determined by *in situ* reflectance spectroscopy. The refractive index value was taken at 600nm. Data obtained before the completion of the nucleation period was ignored. Final film thicknesses after 100 deposition cycles are listed.

4. Conclusions

An *in situ* reflectance spectroscopy tool was developed and implemented with an atmospheric pressure-spatial atomic layer deposition system. A reflectance probe mounted above the deposition stage was able to capture reflectance spectra every two deposition cycles of growing insulating (Al_2O_3) and semiconducting (ZnO) metal oxide thin films. The spectra were fitted to optical reflectance models in real-time to obtain properties such as thickness, refractive index and optical bandgap (for semiconductors). Goodness of fit values for each fitted spectrum were obtained to indicate the level of confidence in the obtained properties.

The approach works well to study the nucleation and property evolution of metal oxide films deposited with this open-air technique. A two-stage growth mechanism was observed, consistent with previous reports of an initial nucleation period to saturate the surface with metal oxide nuclei that eventually grow into a continuous film after which, linear growth occurs. *In-situ* thickness characterization is therefore crucial to enable to the accurate deposition of films with a desired thickness, as linear growth rates cannot be assumed from the start.

The influence of deposition parameters such as substrate oscillation speed, temperature and precursor concentration, on the growth behavior of the films was studied. The length of the nucleation period for ZnO depositions was sensitive to the oscillation speed and temperature. Faster oscillation speeds resulted in a longer nucleation period and higher deposition temperatures shortened the nucleation period, which was consistent with AP-CVD growth. Similarly, a wide range of growth rates were achievable (0.1–3 nm per AP-SALD cycle) by varying the deposition parameters. Furthermore, the high reactivity of pyrophoric precursors deposited in open atmosphere can result in errors that appear as sudden changes in growth rate during a deposition. The real time monitoring of growth rate allows the user to ensure film growth is occurring as expected.

The evolution of optical properties such as bandgap and refractive index of the growing film was observed and followed expected behavior relating to the crystallinity and density of the thin films. It was clear the deposition temperature influenced the optical properties of the film. The bandgap of ZnO films decreased as a function of deposition cycles and increasing temperature. The low bandgap of ZnO obtained at higher deposition temperatures was consistent with reported atmospheric CVD grown ZnO. The trend of increasing Al_2O_3 refractive index as a function of deposition temperature was similar to that of films grown by conventional ALD. An *ex situ* characterization technique such as x-ray photoelectron spectroscopy [10] or ion beam analysis [74, 75] is warranted to study variation in the film's chemical composition and its effect on the optical properties.

The nucleation and property evolution for films deposited with an AP-SALD system has not been studied in detail previously. By implementing *in situ* reflectance spectroscopy, the growth behavior and film properties can be obtained and monitored in real time during a deposition. The observed growth behavior and optical properties of the films were comparable to values reported for atmospheric pressure CVD.

Acknowledgments

K Mistry would like to thank V H Nguyen and D Muñoz-Rojas for sharing their knowledge, guidance and training in the initial stages of this project. K Mistry acknowledges the support of the Mitacs Globalink research

program, Ontario Graduate Scholarship (OGS) and the Natural Sciences and Engineering Research Council of Canada (NSERC). K Mistry and M Kao acknowledge the support of Waterloo Institute for Nanotechnology (WIN) Nanofellowship program. K P Musselman acknowledges the support of the NSERC Discovery Program (RGPIN-2017-04212), and NSERC Discovery Accelerator Supplement (RGPAS-2017-507977). The University of Waterloo's QNFCF facility was used for this work.

Conflicts of interest

There are no conflicts to declare.

Data availability statement

The data that support the findings of this study are available upon reasonable request from the authors.

ORCID iDs

Kissan Mistry https://orcid.org/0000-0001-9593-6896
Alexander Jones https://orcid.org/0000-0003-2270-2698
Kevin P Musselman https://orcid.org/0000-0002-9752-0015

References

[1] Masse de la Huerta C, Nguyen V, Dedulle J-M, Bellet D, Jiménez C and Muñoz-Rojas D 2018 Influence of the geometric parameters on the deposition mode in spatial atomic layer deposition: a novel approach to area-selective deposition *Coatings* **9** 5
[2] Musselman K P, Muñoz-Rojas D, Hoye R L Z, Sun H, Sahonta S L, Croft E, Böhm M L, Ducati C and MacManus-Driscoll J L 2017 Rapid open-air deposition of uniform, nanoscale, functional coatings on nanorod arrays *Nanoscale Horizons* **2** 110–7
[3] Poodt P, Cameron D C, Dickey E, George S M, Kuznetsov V, Parsons G N, Roozeboom F, Sundaram G and Vermeer A 2012 Spatial atomic layer deposition: a route towards further industrialization of atomic layer deposition *J. Vac. Sci. Technol. A Vacuum, Surfaces, Film.* **30** 010802
[4] Muñoz-Rojas D and Macmanus-Driscoll J 2014 Spatial atmospheric atomic layer deposition: a new laboratory and industrial tool for low-cost photovoltaics *Mater. Horizons* **1** 314–20
[5] Hoye R L Z, Muñoz-Rojas D, Nelson S F, Illiberi A, Poodt P, Roozeboom F and Macmanus-Driscoll J L 2015 Research update: Atmospheric pressure spatial atomic layer deposition of ZnO thin films: reactors, doping, and devices *APL Mater.* **3** 040701
[6] Musselman K P, Uzoma C F and Miller M S 2016 Nanomanufacturing: high-throughput, cost-effective deposition of atomic scale thin films via atmospheric pressure spatial atomic layer deposition *Chem. Mater.* **28** 8443–52
[7] Mameli A, Van Den Bruele F J, Ande C K, Verheijen M A, Kessels W M M and Roozeboom F 2016 On the growth, percolation and wetting of silver thin films grown by atmospheric-plasma enhanced spatial atomic layer deposition *ECS Trans.* **75** 129–42
[8] Levy D H, Nelson S F and Freeman D 2009 Oxide electronics by spatial atomic layer deposition *J. Disp. Technol.* **5** 484–94
[9] Illiberi A *et al* 2018 Atmospheric plasma-enhanced spatial-ALD of InZnO for high mobility thin film transistors *J. Vac. Sci. Technol. A Vacuum, Surfaces, Film.* **36** 04F401
[10] Alshehri A H, Mistry K, Nguyen V H, Ibrahim K H, Muñoz-Rojas D, Yavuz M and Musselman K P 2019 Quantum-tunneling metal-insulator-metal diodes made by rapid atmospheric pressure chemical vapor deposition *Adv. Funct. Mater.* **29** 1805533
[11] Poodt P, Lankhorst A, Roozeboom F, Spee K, Maas D and Vermeer A 2010 High-speed spatial atomic-layer deposition of aluminum oxide layers for solar cell passivation *Adv. Mater.* **22** 3564–7
[12] Muñoz-Rojas D, Sun H, Iza D C, Weickert J, Chen L, Wang H, Schmidt-Mende L and MacManus-Driscoll J L 2013 High-speed atmospheric atomic layer deposition of ultra thin amorphous TiO_2 blocking layers at 100 °c for inverted bulk heterojunction solar cells *Prog. Photovoltaics Res. Appl.* **21** 393–400
[13] Hoye R L Z *et al* 2014 Improved open-circuit voltage in ZnO-PbSe quantum dot solar cells by understanding and reducing losses arising from the ZnO conduction band tail *Adv. Energy Mater.* **4** 1–6
[14] Hoffmann L, Brinkmann K O, Malerczyk J, Rogalla D, Becker T, Theirich D, Shutsko I, Görrn P and Riedl T 2018 Spatial atmospheric pressure atomic layer deposition of tin oxide as an impermeable electron extraction layer for perovskite solar cells with enhanced thermal stability *ACS Appl. Mater. Interfaces* **10** 6006–13
[15] Illiberi A, Frijters C, Ruth M, Bremaud D, Poodt P, Roozeboom F and Bolt P J 2018 Atmospheric spatial atomic layer deposition of ZnOS buffer layers for flexible Cu(In,Ga)Se 2 solar cells *J. Vac. Sci. Technol.* A **36** 051511
[16] Hsu C H, Huang C W, Cho Y S, Wu W Y, Wuu D S, Zhang X Y, Zhu W Z, Lien S Y and Ye C S 2019 Efficiency improvement of PERC solar cell using an aluminum oxide passivation layer prepared via spatial atomic layer deposition and post-annealing *Surf. Coatings Technol.* **358** 968–75
[17] Ehrler B, Musselman K P, Böhm M L, Morgenstern F S F F, Vaynzof Y, Walker B J, MacManus-Driscoll J L and Greenham N C 2013 Preventing interfacial recombination in colloidal quantum dot solar cells by doping the metal oxide *ACS Nano* **7** 4210–20
[18] Hoye R L Z, Chua M R, Musselman K P, Li G, Lai M L, Tan Z K, Greenham N C, MacManus-Driscoll J L, Friend R H and Credgington D 2015 Enhanced performance in fluorene-free organometal halide perovskite light-emitting diodes using tunable, low electron affinity oxide electron injectors *Adv. Mater.* **27** 1414–9
[19] Choi H, Shin S, Jeon H, Choi Y, Kim J, Kim S, Chung S C and Oh K 2016 Fast spatial atomic layer deposition of Al_2O_3 at low temperature (<100 °C) as a gas permeation barrier for flexible organic light-emitting diode displays *J. Vac. Sci. Technol. A Vacuum, Surfaces, Film.* **34** 01A121

[20] Di D, Yang L, Richter J M, Meraldi L, Altamimi R M, Alyamani A Y, Credgington D, Musselman K P, MacManus-Driscoll J L and Friend R H 2017 Efficient Triplet Exciton Fusion in Molecularly Doped Polymer Light-Emitting Diodes *Adv. Mater.* **29** 1605987

[21] Nguyen V H, Gottlieb U, Valla A, Muñoz D, Bellet D and Muñoz-Rojas D 2018 Electron tunneling through grain boundaries in transparent conductive oxides and implications for electrical conductivity: The case of ZnO:Al thin films *Mater. Horizons* **5** 715–26

[22] Yousfi E B, Fouache J and Lincot D 2000 Study of atomic layer epitaxy of zinc oxide by *in situ* quartz crystal microgravimetry *Appl. Surf. Sci.* **153** 223–34

[23] Rahtu A, Alaranta T and Ritala M 2001 *In situ* quartz crystal microbalance and quadrupole mass spectrometry studies of atomic layer deposition of aluminum oxide from trimethylaluminum and water *Langmuir* **17** 6506–9

[24] Koster G 2011 Reflection high-energy electron diffraction (RHEED) for *in situ* characterization of thin film growth *In Situ Characterization of Thin Film Growth* ed G Koster and G Rijnders (Cambridge: Woodhead Publishing) 1 pp 3–28 (https://sciencedirect.com/science/article/pii/B9781845699345500011)

[25] Bankras R, Holleman J, Schmitz J, Sturm M, Zinine A, Wormeester H and Poelsema B 2006 *In situ* reflective high-energy electron diffraction analysis during the initial stage of a Trimethylaluminum/Water ALD process *Chem. Vap. Depos.* **12** 275–9

[26] Langereis E, Heil S B S, Knoops H C M, Keuning W, Van De Sanden M C M and Kessels W M M 2009 *In situ* spectroscopic ellipsometry as a versatile tool for studying atomic layer deposition *J. Phys. D: Appl. Phys.* **42** 073001

[27] Mione M A, Engeln R, Vandalon V, Kessels W M M and Roozeboom F 2019 Infrared and optical emission spectroscopy study of atmospheric pressure plasma-enhanced spatial ALD of Al2O3 *Appl. Phys. Lett.* **115** 083101

[28] Yersak A, Lee Y-C, Spencer J and Groner M 2014 Atmospheric pressure spatial atomic layer deposition web coating with *in situ* monitoring of film thickness *J. Vac. Sci. Technol. A Vacuum, Surfaces, Film.* **32** 01A130

[29] Hoye R L Z, Muñoz-Rojas D, Musselman K P, Vaynzof Y and MacManus-Driscoll J L 2015 Synthesis and modeling of uniform complex metal oxides by close-proximity atmospheric pressure chemical vapor deposition *ACS Appl. Mater. Interfaces* **7** 10684–94

[30] Kao M 2018 *An Intelligent Neural Network Controlled Atmospheric Pressure Spatial Atomic Layer Deposition System for Tunable Metal Oxide Thin Films* University of Waterloo (http://hdl.handle.net/10012/13642)

[31] Quinten M 2012 *A Practical Guide to Optical Metrology for Thin Films* (Weinheim, Germany: Wiley-VCH Verlag GmbH & Co. KGaA) 9783527664344 (https://doi.org/10.1002/9783527664344)

[32] Jellison G E and Modine F A 1996 Parameterization of the optical functions of amorphous materials in the interband region *Appl. Phys. Lett.* **69** 371–3

[33] Ferlauto A S, Ferreira G M, Pearce J M, Wronski C R, Collins R W, Deng X and Ganguly G 2002 Analytical model for the optical functions of amorphous semiconductors from the near-infrared to ultraviolet: applications in thin film photovoltaics *J. Appl. Phys.* **92** 2424–36

[34] The Mathworks, Inc. 2018 Solve Nonlinear Curve-Fitting (Data-Fitting) Problems in Least-Square sense - MATLAB lsqcurvefit (https://mathworks.com/help/optim/ug/lsqcurvefit.html)

[35] Yim C, O'Brien M, McEvoy N, Winters S, Mirza I, Lunney J G and Duesberg G S 2014 Investigation of the optical properties of MoS_2 thin films using spectroscopic ellipsometry *Appl. Phys. Lett.* **104** 103114

[36] Tauc J 1968 Optical properties and electronic structure of amorphous Ge and Si *Mater. Res. Bull.* **3** 37–46

[37] Maiti U N, Ghosh P K, Nandy S and Chattopadhyay K K 2007 Effect of Mn doping on the optical and structural properties of ZnO nano/micro-fibrous thin film synthesized by sol-gel technique *Phys. B Condens. Matter* **387** 103–8

[38] Guo M, Yang C Y, Zhang M, Zhang Y J, Ma T, Wang X D X D X X X X D and Wang X D X D X X X X D 2008 Effects of preparing conditions on the electrodeposition of well-aligned ZnO nanorod arrays *Electrochim. Acta* **53** 4633–41

[39] Caglar M, Ilican S, Caglar Y and Yakuphanoglu F 2009 Electrical conductivity and optical properties of ZnO nanostructured thin film *Appl. Surf. Sci.* **255** 4491–6

[40] Fujiwara H, Koh J, Rovira P I and Collins R W 2000 Assessment of effective-medium theories in the analysis of nucleation and microscopic surface roughness evolution for semiconductor thin films *Phys. Rev.* B **61** 10832–44

[41] Massoudi I, Habchi M M, Rebey A and El Jani B 2012 Study of surface roughness using spectral reflectance measurements recorded during the MOVPE of InAs/GaAs heterostructures *Phys. E Low-Dimensional Syst. Nanostructures* **44** 1282–7

[42] Franta D and Ohlídal I 2005 Comparison of effective medium approximation and Rayleigh-Rice theory concerning ellipsometric characterization of rough surfaces *Opt. Commun.* **248** 459–67

[43] Lim J, Shin K, Kim H and Lee C 2005 Enhancement of ZnO nucleation in ZnO epitaxy by atomic layer epitaxy *Thin Solid Films* **475** 256–61

[44] Baji Z, Lábadi Z, Horváth Z E, Molnár G, Volk J, Bársony I and Barna P 2012 Nucleation and growth modes of ALD ZnO *Cryst. Growth Des.* **12** 5615–20

[45] Makino H, Kishimoto S, Yamada T, Miyake A, Yamamoto N and Yamamoto T 2008 Effects of surface pretreatment on growth of ZnO on glass substrate *Phys. Status Solidi Appl. Mater. Sci.* **205** 1971–4

[46] Puurunen R L 2005 Surface chemistry of atomic layer deposition: a case study for the trimethylaluminum/water process *J. Appl. Phys.* **97** 121301

[47] Biswas C, Ma Z, Zhu X, Kawaharamura T and Wang K L 2016 Atmospheric growth of hybrid ZnO thin films for inverted polymer solar cells *Sol. Energy Mater. Sol. Cells* **157** 1048–56

[48] Hu J and Gordon R G 1992 Textured aluminum-doped zinc oxide thin films from atmospheric pressure chemical-vapor deposition *J. Appl. Phys.* **71** 880–90

[49] Guziewicz E *et al* 2009 ZnO grown by atomic layer deposition: a material for transparent electronics and organic heterojunctions *J. Appl. Phys.* **105** 122413

[50] Illiberi A, Roozeboom F and Poodt P 2012 Spatial atomic layer deposition of zinc oxide thin films *ACS Appl. Mater. Interfaces* **4** 268–72

[51] Ratzsch S, Kley E, Tünnermann A and Szeghalmi A 2015 Influence of the oxygen plasma parameters on the atomic layer deposition of titanium dioxide *Nanotechnology* **26** 024003

[52] Janocha E and Pettenkofer C 2011 ALD of ZnO using diethylzinc as metal-precursor and oxygen as oxidizing agent *Appl. Surf. Sci.* **257** 10031–5

[53] Johnson R W, Hultqvist A and Bent S F 2014 A brief review of atomic layer deposition: from fundamentals to applications *Mater. Today* **17** 236–46

[54] Tan S, Yang W, Kanarik K J, Lill T, Vahedi V, Marks J and Gottscho R A 2015 Highly selective directional atomic layer etching of silicon *ECS J. Solid State Sci. Technol.* **4** N5010–2

[55] Oehrlein G S, Metzler D and Li C 2015 Atomic layer etching at the tipping point: an overview *ECS J. Solid State Sci. Technol.* **4** N5041–53

[56] Nasution I, Velasco A and Kim H J 2009 Atmospheric pressure chemical vapor deposition mechanism of Al_2O_3 film from $AlCl_3$ and O_2 *J. Cryst. Growth* **311** 429–34

[57] Muñoz-Rojas D, Nguyen V H, Masse de la Huerta C, Aghazadehchors S, Jiménez C and Bellet D 2017 Spatial atomic layer deposition (SALD), an emerging tool for energy materials. Application to new-generation photovoltaic devices and transparent conductive materials *Comptes Rendus Phys.* **18** 391–400
[58] Jur J S and Parsons G N 2011 Atomic layer deposition of Al_2O_3 and ZnO at atmospheric pressure in a flow tube reactor *ACS Appl. Mater. Interfaces* **3** 299–308
[59] Mousa M B M, Oldham C J and Parsons G N 2014 Atmospheric pressure atomic layer deposition of Al_2O_3 using trimethyl aluminum and ozone *Langmuir* **30** 3741–8
[60] Caglar M, Caglar Y, Aksoy S and Ilican S 2010 Temperature dependence of the optical band gap and electrical conductivity of sol-gel derived undoped and Li-doped ZnO films *Appl. Surf. Sci.* **256** 4966–71
[61] Allen P B and Heine V 1976 Theory of the temperature dependence of electronic band structures *J. Phys. C: Solid State Phys.* **9** 2305–12
[62] Nguyen V H, Resende J, Jiménez C, Deschanvres J L, Carroy P, Muñoz D, Bellet D and Muñoz-Rojas D 2017 Deposition of ZnO based thin films by atmospheric pressure spatial atomic layer deposition for application in solar cells *J. Renew. Sustain. Energy* **9** 021203
[63] Marotti R E, Giorgi P, Machado G and Dalchiele E A 2006 Crystallite size dependence of band gap energy for electrodeposited ZnO grown at different temperatures *Sol. Energy Mater. Sol. Cells* **90** 2356–61
[64] Vorobiev Y V, Horley P P, Hernández-Borja J, Esparza-Ponce H E, Ramírez-Bon R, Vorobiev P, Pérez C and González-Hernández J 2012 The effects of porosity on optical properties of semiconductor chalcogenide films obtained by the chemical bath deposition *Nanoscale Res. Lett.* **7** 483
[65] Sagnes I, Halimaoui A, Vincent G and Badoz P A 1993 Optical absorption evidence of a quantum size effect in porous silicon *Appl. Phys. Lett.* **62** 1155–7
[66] Luka G, Krajewski T, Wachnicki L, Witkowski B, Lusakowska E, Paszkowicz W, Guziewicz E and Godlewski M 2010 Transparent and conductive undoped zinc oxide thin films grown by atomic layer deposition *Phys. Status Solidi Appl. Mater. Sci.* **207** 1568–71
[67] Iqbal J, Jilani A, Ziaul Hassan P M, Rafique S, Jafer R and Alghamdi A A 2016 ALD grown nanostructured ZnO thin films: effect of substrate temperature on thickness and energy band gap *J. King Saud Univ. - Sci.* **28** 347–54
[68] Varshni Y P 1967 Temperature dependence of the energy gap in semiconductors *Physica* **34** 149–54
[69] Maleki M and Rozati S M 2015 Dependence of ZnO nanostructured thin films properties on growth temperature by APCVD method *Acta Phys. Pol.* A **128** 367–72
[70] Ellinger C R and Nelson S F 2014 Selective area spatial atomic layer deposition of ZnO, Al_2O_3, and aluminum-doped ZnO using Poly (vinyl pyrrolidone) *Chem. Mater.* **26** 1514–22
[71] Groner M D, Fabreguette F H, Elam J W and George S M 2004 Low-temperature $Al2O_3$ atomic layer deposition *Chem. Mater.* **16** 639–45
[72] Kukli K, Ritala M, Leskelä M and Jokinen J 1997 Atomic layer epitaxy growth of aluminum oxide thin films from a novel Al(CH3)2Cl precursor and H_2O *J. Vac. Sci. Technol. A Vacuum, Surfaces, Film.* **15** 2214–8
[73] Poodt P, Knaapen R, Illiberi A, Roozeboom F and van Asten A 2012 Low temperature and roll-to-roll spatial atomic layer deposition for flexible electronics *J. Vac. Sci. Technol. A Vacuum, Surfaces, Film.* **30** 01A142
[74] Baron-Wiecheć A, Burke M G, Hashimoto T, Liu H, Skeldon P, Thompson G E, Habazaki H, Ganem J-J and Vickridge I C 2013 Tracer study of pore initiation in anodic alumina formed in phosphoric acid *Electrochim. Acta* **113** 302–12
[75] Amsel G and Samuel D 1967 Microanalysis of the stable isotopes of oxygen by means of nuclear reactions *Anal. Chem.* **39** 1689–98